

Motion and Context-Aware Audio-Visual Conditioned Video Prediction

Yating Xu^{a,**}, Gim Hee Lee^a

^aSchool of Computing, National University of Singapore, Singapore 117417, Republic of Singapore

arXiv:2212.04679v1 [cs.CV] 9 Dec 2022

ABSTRACT

Existing state-of-the-art method for audio-visual conditioned video prediction uses the latent codes of the audio-visual frames from a multimodal stochastic network and a frame encoder to predict the next visual frame. However, a direct inference of per-pixel intensity for the next visual frame from the latent codes is extremely challenging because of the high-dimensional image space. To this end, we propose to decouple the audio-visual conditioned video prediction into motion and appearance modeling. The first part is the multimodal motion estimation module that learns motion information as optical flow from the given audio-visual clip. The second part is the context-aware refinement module that uses the predicted optical flow to warp the current visual frame into the next visual frame and refines it based on the given audio-visual context. Experimental results show that our method achieves competitive results on existing benchmarks.

© 2022 Elsevier Ltd. All rights reserved.

1. Introduction

Human perceive the world via multisensory processing. Particularly, audio-visual interactions are ubiquitous in our daily life. Imagine you are at the bus stop where you hear and see the bus approaching, but your vision is suddenly obscured by another pedestrian. Nonetheless, your brain is still able to fill in the missing visual content based on the visual frames seen previously and the complete audio information. It has also been proven in neurobiology studies that such audio-visual pairing has the advantage of increasing the activation of neurons (Knöpfel et al., 2019) to enhance perceptual ability. Inspired by these observations, we focus our study of audio-visual interaction on the task of audio-visual conditioned video prediction.

Fig. 1 shows an illustration of the task of audio-visual conditioned video prediction. Given a full audio clip and a short sequence of the past visual frames, the objective is to predict the missing future visual frames that are as close to the ground truth frames as possible. The given audio clips and visual frames act as a guidance in predicting the motion and appearance of future visual frames.

Existing state-of-the-art work Sound2Sight (Chatterjee and Cherian, 2020) proposes to directly infer per-pixel intensity

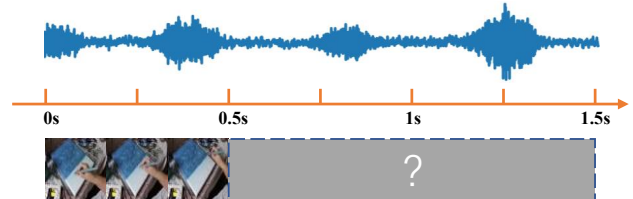


Fig. 1. An illustration of audio-visual conditioned video prediction task. Given full audio clip and a short sequence of past visual frames, we aim to predict corresponding future visual frames.

of future images from the audio-visual inputs. A multimodal stochastic network is used to encode the audio-visual frames into a latent space distribution. Subsequently, a random vector is drawn from this latent space distribution to capture multiple plausible futures. This random vector is then concatenated with the embedding of the current visual frame to predict the next visual frame. However, a direct inference of the per-pixel intensity for the next visual frame from the latent codes is extremely challenging because of the high-dimensional image space. As a result, Sound2Sight can fail to preserve the visual content in the generated visual frames. Fig. 2 shows an example on the MovingMNIST data, where Sound2Sight generates a wrong digit despite the correct motion of the generated moving digit. We postulate that this inability to preserve the visual content, *i.e.* the appearance of the digit, but yet a correct prediction of the mo-

**Corresponding author:

e-mail: xu.yating@u.nus.edu (Yating Xu)

	t=15									
	t=6									
GT	8	8	8	8	8	8	8	8	8	8
Sound2Sight	0	0	0	0	0	0	0	0	0	0
Our Method	8	8	8	8	8	8	8	8	8	8

Fig. 2. Example of wrong content predictions from Sound2Sight (Chatterjee and Cherian, 2020) (second row) vs. the correct predictions from our method (last row) compared with the ground truth (top row) on the Mov-MNIST data.

tion is caused by the tightly entangled appearance and motion modeling in Sound2Sight.

In consideration of the above-mentioned limitation of Sound2Sight, we decouple video prediction into two distinct components of motion and appearance. Given the audio-visual prior information, we first predict the movements of the objects in the future frames as optical flow, *i.e.* motion. We then use the predicted optical flow to warp the current visual frame into the next visual frame followed by a refinement module to fill-in the missing regions and to improve the visual quality, *i.e.* appearance. In contrast to the direct per-pixel intensity estimation from the latent codes in Sound2Sight, our two-stage strategy is capable of preventing grossly wrong content prediction since we rely on optical flow to warp the current frame into the next visual frame. Furthermore, both stages of our framework are conditioned on the given audio clips to ensure the fidelity of the generated visual frames with its corresponding audio clip.

More concretely, our proposed framework consists of two modules: 1) multimodal motion estimation and 2) context-aware refinement for motion and appearance, respectively. Our multimodal motion estimation module consists of the audio and visual branches. The audio branch extracts audio features from the input audio samples. We then apply self-attention on the extracted features and store the output features in a motion memory. The visual branch recalls corresponding motion information from the motion memory via a querying step similar to cross-attention. These recalled features are passed into a convolutional LSTM and a motion decoder to predict the optical flow between the current and next frame. Our context-aware refinement network recurrently renders the next visual frame by warping the current frame with the predicted optical flow. However, this recurrent warping eventually causes the predicted visual frames to become blurry and lose contextual information. To mitigate these problem, we design a context encoder to encode the global appearance information from the last given visual frame. This encoded feature is then combined with the predicted motion and given audio features of the next frame as an additional input to the rendering network.

We further observe that existing benchmarks contains a large portion of videos with small or no motions. This means that a model can achieve good results by simply copying last ground truth image. To avoid such shortcut and better evaluate the ability of a model to predict motions, it is important to exclude such video segments. Therefore, we select a subset of videos with clear motion as an additional benchmark.

Our contributions in this paper are as follows:

- We address the task of audio-visual conditioned video pre-

diction by decomposing it into motion and appearance. Our proposed approach relies on optical flow to warp the current frame into the next frame, and thus can avoid grossly wrong content prediction.

- We propose the multimodal motion estimation module to predict optical flow of the next visual frame by storing the audio features into a motion memory. We design the Condense and Recall operators to effectively utilize this motion memory.
- We propose the context-aware refinement module to render the next predicted visual frame. We design a novel context encoder that works together with the motion and audio encoders to mitigate the loss of global context in long term predictions of the visual frames.
- We observe that large portions of existing benchmarks videos consist of small or no motion. For better evaluation, we select subsets of videos with clear motion. Experiments show our model achieves competitive results on all benchmarks.

2. Related Work

Video prediction. Video prediction aims to predict video frames close to ground truth future frames conditioned on a few past frames. It can be divided into two categories: prediction in pixel space (Wang et al., 2017; Jin et al., 2020; Xingjian et al., 2015; Lee et al., 2021a; Wang et al., 2018b), and prediction in low-dimensional space (Lee et al., 2021b; Villegas et al., 2017, 2018; Wu et al., 2020). Prediction in pixel space refers to direct estimation of per-pixel intensity. PredRNN (Wang et al., 2017) enables memory states to be updated across vertically stacked RNN layers and horizontally through all RNN states. E3D-LSTM (Wang et al., 2018b) introduce a memory recall mechanism inside a LSTM to encode long-term information. Jin et al. (2020) adopt multi-level wavelet transform to deal with motion blur and missing appearance details. Lee et al. (2021a) deal with long-term motion context by building a long-term motion context memory. It uses memory alignment learning to enable network to recall long-term motion context corresponds to input sequence. Besides, several works (Denton and Fergus, 2018; Lee et al., 2018) consider stochasticity in the prediction by learning a prior distribution to capture the future dynamics.

Direct estimation of per-pixel intensity of future visual frames is a very challenging task because of the high-dimensional image space. As a result, there are many works that seek to predict a low-dimensional representation and then translate it into the future visual frames. Lee et al. (2021b) propose a two-stage prediction by first predicting future semantic maps and then generate future frames conditioned on the context frames and output of the first stage via video-to-video synthesis (Wang et al., 2018a). Villegas et al. (2017) first predict future human pose before generating future images via visual analogy (Reed et al., 2015). Villegas et al. (2018) further propose a hierarchical prediction without ground truth annotations

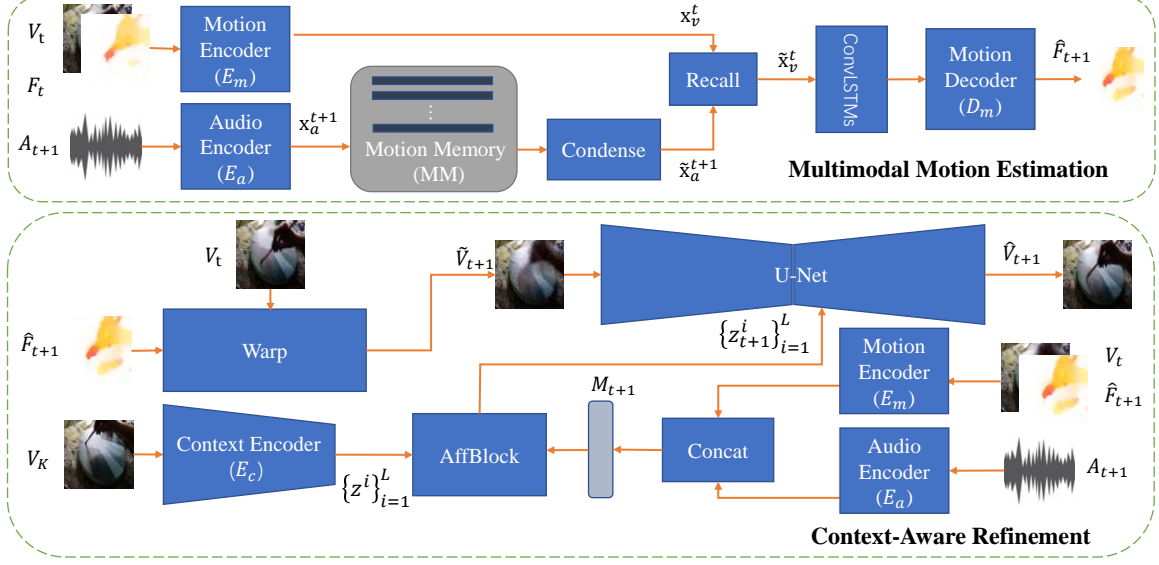


Fig. 3. Our framework consists of the Multimodal Motion Estimation (MME) and Context-Aware Refinement (CAR) modules. MME uses the given audio-visual information to predict motion as optical flow. Subsequently, CAR first uses the predicted optical flow to warp the current visual frame into the next predicted frame and then refines it with the given audio-visual context.

for low-dimensional data. It constrains the predicted feature to be close to the outputs of a future encoder. Bei et al. (2021) first infer future optical flow and semantic labels independently for each object in the scene and then use U-Net (Ronneberger et al., 2015) to inpaint the future images.

We share the same problem setting as Sound2Sight (Chatterjee and Cherian, 2020). They learn a joint audio-visual latent embedding to capture future dynamics. However, the latent codes cause the tight entanglement of motion and appearance, and thus making it difficult for the model to balance the capture of correct motion and maintaining the shape of objects. Our solution is to decouple audio-visual conditioned video prediction into two components by modeling motion and appearance separately.

Audio-visual representation learning. Audio-Visual representation learning aims to learn a general representation in a self-supervised way by utilizing audio-visual correlation. There are mainly three types of correspondences: semantic similarity (Arandjelovic and Zisserman, 2017; Aytar et al., 2016; Arandjelovic and Zisserman, 2018; Hu et al., 2019; Morgado et al., 2021), temporal consistency (Owens and Efros, 2018; Korbar et al., 2018; Afouras et al., 2020) and spatial correspondence (Gao et al., 2020; Yang et al., 2020). Arandjelovic and Zisserman (2017) propose audio-visual correspondence learning by classifying whether the input audio and visual frame are from the same video or not. Owens and Efros (2018) design a pretext task to predict whether audio stream and visual sequence are temporally aligned. Yang et al. (2020) leverage audio-visual spatial correspondence by predicting whether the two channels of audio are flipped. In addition to learning a general representation, there are also many variants of audio-visual tasks, such as sound source localization (Chen et al., 2021; Senocak et al., 2018; Hu et al., 2020), audio-visual source separation (Gao and Grauman, 2019; Zhao et al., 2018, 2019), audio-visual video

parsing (Tian et al., 2020; Wu and Yang, 2021) and talking face generation (Chung et al., 2017; Zhou et al., 2019; Chen et al., 2019; Vougioukas et al., 2018). In this paper, we study the task of audio-visual conditioned video prediction by leveraging audio-motion correlation.

3. Method

Problem definition. Let us denote a video with T frames as $\mathcal{V} = \{V_1, A_1\}, \dots, \{V_T, A_T\}$, where $\{V_t, A_t\}$ represents a visual frame V_t and its corresponding audio clip A_t . A visual frame V_t is an image of size $C \times W \times H$, where C is the number of channels, W and H are the width and height of the image. An audio clip A_t is a $\mathcal{F} \times \mathcal{T}$ two-dimensional spectrogram, where \mathcal{F} denotes the frequency range and \mathcal{T} represents the time duration of the audio clip. Given the first K visual frames $\{V_1, \dots, V_K\}$ and the whole audio $\{A_1, \dots, A_T\}$, the goal of the audio-visual conditioned video prediction task is to predict the missing $T - K$ visual frames $\{V_{K+1}, \dots, V_T\}$ to be as similar to the ground truth visual frames as possible. For brevity, we drop the frame index K and denote the indices of the previous, current and next predicted frames as $t - 1$, t and $t + 1$, respectively.

Method overview. Fig. 3 shows our proposed framework which consists of two modules: 1) multimodal motion estimation (MME) and 2) context-aware refinement (CAR). Our MME and CAR modules are designed to model motion and context, respectively. Specifically, our MME predicts the optical flow \hat{F}_{t+1} between the current visual frame V_t and next visual frame \hat{V}_{t+1} from the next audio clip A_{t+1} , and current visual frame V_t and optical flow F_t . An audio and a visual branch process the audio and visual inputs, respectively. In the audio branch, we store the audio feature x_a^{t+1} into a motion memory since audio conveys a clear motion cue. For example, the rhythm of the sound corresponds to the tempo of a moving

brush. The motion memory outputs a condensed motion memory feature \tilde{x}_a^{t+1} via self-attention. The visual branch recalls relevant motion information from \tilde{x}_a^{t+1} . We send the enhanced motion feature \tilde{x}_v^t into ConvLSTMs (Xingjian et al., 2015) to predict next optical flow \hat{F}_{t+1} . Subsequently, we predict the next visual frame \hat{V}_{t+1} with the predicted optical flow \hat{F}_{t+1} using CAR. We start by warping the current visual frame V_t using the predicted optical flow to get a coarse prediction of the next visual frame \hat{V}_{t+1} followed by a refinement by a U-Net to get the final predicted visual frame \hat{V}_{t+1} . To mitigate the loss of appearance context, we add a context encoder to extract the global appearance context feature Z from the last given visual frame V_K . The global appearance context feature Z is then fed into the motion-conditioned affine transformation with the concatenated features from V_t , \hat{F}_{t+1} and A_{t+1} to get the transformed context feature Z_{t+1} . Finally, Z_{t+1} is used as a appearance context condition on the U-Net decoder to predict the next visual frame \hat{V}_{t+1} .

3.1. Multimodal Motion Estimation

The MME predicts optical flow in a recurrent way. For ease of warping, the MME operates on backward optical flow, *i.e.* both input F_t and output \hat{F}_{t+1} are backward optical flow. We use both audio and visual modalities in this module because they both contain clear motion information. To make prediction of the $t+1$ frame, the motion encoder E_m takes the concatenation of the current optical flow F_t and visual frame V_t as inputs, and outputs the motion feature $x_v^t \in \mathbb{R}^{w \times h \times c}$. Note that V_t is a given visual frame if $t \leq K$, otherwise it is V_{t-1} warped by the predicted optical flow F_t . We do not refine the warped image in MME. Concurrently, the audio encoder E_a outputs the audio feature $x_a^{t+1} \in \mathbb{R}^c$ from input audio signal A_{t+1} .

It is important to ensure that there is long-term memory for the audio information in our recurrent MME for it to play an effective role in motion prediction. However, the obvious choice of LSTM is notorious for only have short memory, where the memory cell quickly saturated to remember only the latest input. As a result, it is difficult to infer long-term future motions. We design an external motion memory MM from the audio features. In contrast to the memory cell inside LSTM that selectively remember past memory, our motion memory MM simply keeps all past memory without abandon. Our advantage is that it does not lose any past memory, and thus efficiently keeps all long-term information. The MM stores audio features up to time $t+1$, $MM = \{x_a^n\}_{n=1}^{t+1} \in \mathbb{R}^{t \times c}$. Visual features recall from MM via cross-attention as the query (**Q**), and MM is used to get the key (**K**) and value (**V**). The size of MM increases linearly with the prediction length, making it difficult for the visual branch to catch useful information from the large memory. Thus, we address this motion memory complexity problem by performing self-attention on the motion memory. We design two operators Condense and Recall as follows:

$$\begin{aligned} \text{Atten}(\mathbf{Q}, \mathbf{K}, \mathbf{V}) &= \text{Softmax}(\mathbf{Q}\mathbf{K}^\top) \mathbf{V}, \\ \text{Condense}(MM) &= \text{Atten}(MM, MM, MM), \\ \text{Recall}(x_v^t, \tilde{x}_a^{t+1}) &= \text{Atten}(x_v^t, \tilde{x}_a^{t+1}, \tilde{x}_a^{t+1}), \end{aligned} \quad (1)$$

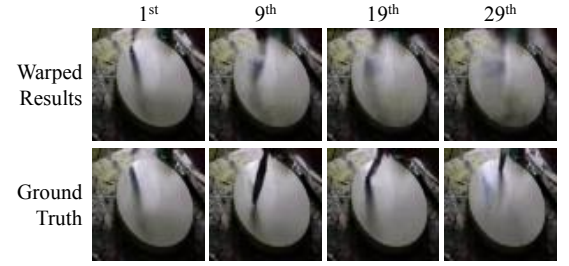


Fig. 4. Example of the warped images. Resultant images become increasingly blurry under recurrent warpings.

where Condense performs self-attention on motion memory MM and Recall performs cross-attention between motion feature x_v^t and condensed motion memory \tilde{x}_a^{t+1} . The condensed motion memory \tilde{x}_a^{t+1} is obtained as follow:

$$\tilde{x}_a^{t+1} = x_a^{t+1} + W_z^c \cdot \text{Condense}(MM)[-1], \quad (2)$$

where W_z^c is the projection weight and $[-1]$ denotes the last slice of the memory. The visual branch then recalls from \tilde{x}_a^{t+1} and obtain the enhanced motion feature as follow:

$$\tilde{x}_v^t = x_v^t + W_z^r \cdot \text{Recall}(x_v^t, \tilde{x}_a^{t+1}), \quad (3)$$

where W_z^r is the projection weight. We further feed \tilde{x}_v^t into ConvLSTMs to predict optical flow at next time step. Unlike LSTM which operates on 1D vectors, ConvLSTM operates on 2D feature maps so that it preserves spatial location. The output of ConvLSTMs is further sent into the motion decoder D_m to predict the optical flow \hat{F}_{t+1} as follow:

$$\begin{aligned} \{h_{t+1}, o_{t+1}\} &= \text{ConvLSTM}(\tilde{x}_v^t, h_t), \\ \hat{F}_{t+1} &= D_m(h_{t+1}), \end{aligned} \quad (4)$$

where h_{t+1} is the hidden state and o_{t+1} is the cell state of the ConvLSTMs at time step $t+1$.

3.2. Context-Aware Refinement

The Context-Aware Refinement (CAR) module is responsible to produce the next visual frame from the predicted optical flow. It targets at modeling images appearance. Since audio cannot convey any local pixel information, we rely on the visual modality for appearance information. We start by warping the current visual frame using the predicted optical flow \hat{F}_{t+1} . We then adopt bilinear interpolation (Jaderberg et al., 2015) to warp V_t as follows:

$$\hat{V}_{t+1}(p) = V_t(p + \hat{F}_{t+1}(p)), \quad (5)$$

where p is the pixel coordinates. Similar to MME, note that V_t is a given visual frame if $t \leq K$, otherwise it is the output of CAR from the previous time step.

The warping procedure is performed recurrently by taking current prediction as input and warping it into the next frame. However, this recurrent warping operation causes the warped image become increasingly blurry and consequently leads to the loss of appearance as shown in Fig. 4. It can be seen that

warping at the first time step can provide relatively good result. The warped image gradually becomes blurry, where the shape of the brush and background region are distorted.

To alleviate the blurry visual frame problem, we use a U-Net (Ronneberger et al., 2015) to refine the local details. Furthermore, we add a novel context encoder E_c to extract global appearance context $Z = \{z^i\}_{i=1}^L$ from the last given visual frame V_K . $z^i \in \mathbb{R}^{c^i \times h^i \times w^i}$ is the feature at the i -th layer of E_c . The total layers of features is denoted by L , and it is set as a hyper-parameter. The context encoder resembles the U-Net encoder except that it is shallower. However, the global context may not adapt to the image appearance at each individual step due to motion variance. Inspired by the success of text-image fusion using affine transformation (Tao et al., 2020), we perform motion-conditioned affine transformation to include global context. The transformation parameters $\gamma_{t+1}^i \in \mathbb{R}^c$ and $\beta_{t+1}^i \in \mathbb{R}^c$ for the context features from the i -th layer are obtained from two separate MLPs, which are conditioned on motion feature M_{t+1} so that the transformed feature is able to adapt to motion variance:

$$\gamma_{t+1}^i = \text{MLP}_1^i(M_{t+1}), \quad \beta_{t+1}^i = \text{MLP}_2^i(M_{t+1}). \quad (6)$$

We use the motion encoder E_m and audio encoder E_a from MME to compute the motion feature M_{t+1} as follow:

$$M_{t+1} = \text{Concat}(E_m(V_t, \hat{F}_{t+1}), E_a(A_t)), \quad (7)$$

where $\text{Concat}(\cdot, \cdot)$ denotes the concatenation operation. We use audio to compute M_{t+1} because audio contains motion but not appearance cue. We then perform channel-wise scaling and shifting on z^i to obtain the adapted context z_{t+1}^i :

$$z_{t+1}^i = \gamma_{t+1}^i \cdot z^i + \beta_{t+1}^i. \quad (8)$$

Each AffBlock in Fig. 3 contains twice motion-conditioned affine transformation. Finally, we insert z_{t+1}^i into its corresponding layer in the U-Net decoder.

3.3. Optimization

We train our model in two stages. We optimize MME in the first stage, and then we fix MME and optimize CAR in the second stage. We train MME by optimizing an optical flow reconstruction loss $\mathcal{L}_{\text{flow}}$ and a smoothness regularization term $\mathcal{L}_{\text{smooth}}$:

$$\mathcal{L}_{\text{MME}} = \mathcal{L}_{\text{flow}} + \lambda_{\text{smooth}} \mathcal{L}_{\text{smooth}}, \quad (9)$$

where λ_{smooth} is a weighting hyperparameter for $\mathcal{L}_{\text{smooth}}$. $\mathcal{L}_{\text{flow}}$ computes mean-squared error between the predicted optical flow and ground truth optical flow as follow:

$$\mathcal{L}_{\text{flow}} = \sum_{t=K+1}^T \|F_t - \hat{F}_t\|_2^2. \quad (10)$$

Following (Wu et al., 2020; Yin and Shi, 2018), we have a smoothness regularization term $\mathcal{L}_{\text{smooth}}$ for our optical flow estimation:

$$\mathcal{L}_{\text{smooth}} = \sum_{t=K+1}^T \|\nabla \hat{F}_t\|_1 e^{-\|\nabla V_t\|_1}, \quad (11)$$

where ∇ is the gradient operator. The smoothness loss is weighted by the image gradient to preserve edges in the image.

The supervision for CAR is an image reconstruction loss \mathcal{L}_v , which computes mean-squared error between the predicted and ground truth frames:

$$\mathcal{L}_v = \sum_{t=K+1}^T \|V_t - \hat{V}_t\|_2^2. \quad (12)$$

4. Experiments

Datasets. We conduct experiments on both synthetic and real world datasets taken from (Chatterjee and Cherian, 2020): 1)

Multimodal MovingMNIST. This dataset is an extension of stochastic MovingMNIST (Srivastava et al., 2015) by adding artificial sound. Although MovingMNIST is synthetic, it is a standard benchmark in video prediction (Wang et al., 2018b; Lee et al., 2021a; Denton and Fergus, 2018). In Multimodal MovingMNIST, each digit is equipped with a unique tone and the amplitude of the tone is inversely proportional to the distance of the digit from the origin. The sound changes momentarily whenever the digit hits the boundary. This dataset consists of 8,000 training, and 1,000 test videos. 2) **YouTube Painting.** This dataset contains painting videos from YouTube. In each video, a painter is painting on a canvas in an indoor environment and there is a clear sound of the brush strokes. It contains 4.8 K training, and 500 test videos. Each video is of 64×64 resolution, 30fps, and 3 seconds long. 3) **AudioSet-Drums.** This dataset contains selected videos from the drums class of AudioSet (Gemmeke et al., 2017). The video clips are selected such that the drum player is visible when the drum beat is audible. It contains 6 K training, and 1 K test videos. Each video is of 64×64 resolution, 30fps, and 3 seconds long.

Implementation. The video frames are resized to 48×48 in Multimodal MovingMNIST and 64×64 in YouTube Pianting and Audio-Drums. The intensity value of the video frames are normalized into $[0, 1]$. We directly use the precomputed spectrogram by (Chatterjee and Cherian, 2020) as audio input. We use the Adam optimizer (Kingma and Ba, 2014) and the learning rate is set to $1e-4$ and $1e-3$ for MME and CAR, respectively. The coefficient λ_{smooth} is set to 0.01. We use a 2-layer ConvLSTMs for Multimodal MovingMNIST and a 4-layer ConvLSTMs for the other two datasets. In CAR, we insert $L = 1$ layer context feature for Multimodal MovingMNIST and $L = 4$ layers for the other two datasets. Ground truth optical flow is precomputed using the TV-L1 algorithm from (Zach et al., 2007). We implement our framework with Pytorch on two Nvidia GeForce GTX1080Ti GPUs.

Evaluation setup. On Multimodal MovingMNIST, we show 5 initial frames and full audio, and we predict next 15 frames during training and 20 frames during evaluation. On YouTube Painting and AudioSet-Drums, we show 15 initial visual frames and full audio, and predict next 15 visual frames during training and 30 visual frames during evaluation. We evaluate our method by the structure similarity (SSIM) (Wang et al., 2004) and Peak Signal to Noise Ratio (PSNR). We report SSIM and PSNR on selected visual frames. The mean SSIM and PSNR of

Method	Type	SSIM ↑				PSNR ↑			
		Fr 6	Fr 15	Fr 25	Mean	Fr 6	Fr 15	Fr 25	Mean
Vougioukas et al. (2018)	M	0.8600	0.8571	0.8573	—	15.17	14.99	15.01	—
Denton and Fergus (2018)	V	0.9265	0.8300	0.7999	—	18.59	14.65	13.98	—
Sound2Sight (Chatterjee and Cherian, 2020) *	M	0.9575	0.8943	0.8697	—	21.69	17.62	16.84	—
Sound2Sight (Chatterjee and Cherian, 2020) †	M	0.9505	0.8780	0.8749	0.8910	22.22	18.16	17.84	18.70
Our Method	M	0.9608	0.9158	0.8990	0.9195	23.61	19.88	18.99	20.23

Table 1. Comparison on Multimodal MovingMNIST with 5 seen frames. Higher values are better for SSIM and PSNR. Best results are marked in bold. Type M denotes method using audio-visual modality and Type V denotes only using visual modality. * denotes highest results from 100x sampling reported in (Chatterjee and Cherian, 2020). † denotes our reproduced average results of (Chatterjee and Cherian, 2020) from 100x sampling.

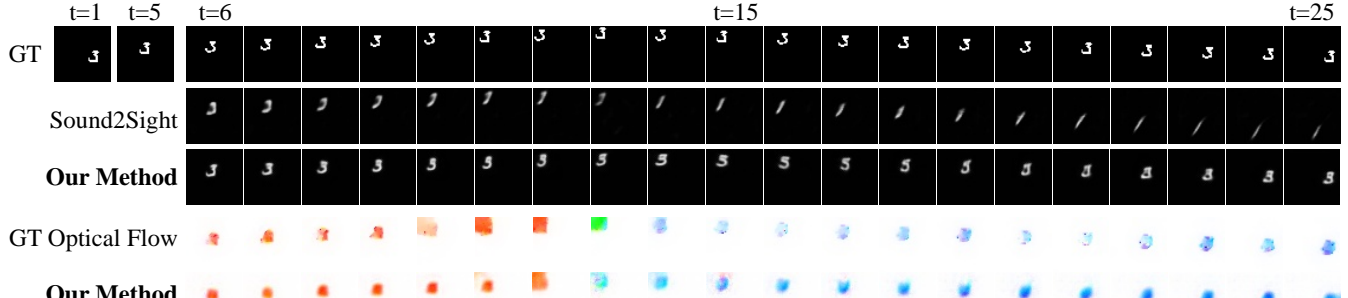


Fig. 5. Qualitative results on Multimodal MovingMNIST.

full predicted sequence are also reported to represent average performance.

4.1. Results

We compare our results with Sound2Sight (Chatterjee and Cherian, 2020), Vougioukas et al. (2018) and Denton and Fergus (2018). We use the reported results from Chatterjee and Cherian (2020). In addition to the best result of the samples drawn from the Sound2Sight model, we also re-run their source code to compute its average score over 100 times of sampling. In practice, it is statistically more meaningful to use the mean instead of the best result since the stochastic approach cannot always achieve the highest result in every sampling. Moreover, we do not know the ground truths of the future visual frames. Therefore, it is unreasonable for (Chatterjee and Cherian, 2020) to search for the best samples drawn from their stochastic model using the ground truths.

Multimodal MovingMNIST. Tab. 1 shows quantitative results on Multimodal MovingMNIST. Our method outperforms others by a large margin across all time steps. Fig. 5 shows the quantitative results. The first three rows show comparison of the predicted visual frames sequence. The last two rows show the corresponding optical flow results. We follow the flow color coding of (Baker et al., 2011). It can be seen that our method is able to correctly predict the trajectory and also maintain the complex shape of digit ‘3’ in long term prediction. On the contrary, the predicted sequence from Sound2Sight gradually loses the shape of the digit and deviates from the correct trajectory.

YouTube Painting. Tab. 2 shows quantitative results on YouTube Painting. Our model again is able to surpass other methods. Fig. 6 shows qualitative comparison with

Sound2Sight. Due to entangled modeling of motion and appearance, the result of Sound2Sight gradually loses the shape of the hand. Furthermore, the hand becomes stationary at the top right corner of the image. In contrast, our model maintains a relatively good appearance and generally follows the movement of hand in ground truth frames. We can also see that our predicted optical flows is close to the ground truths. During experiments, we find there are a large portion of test videos with little or no motion. As a result, the model is still able to achieve very high results by simply copying last ground truth past frame (Copy Last GT). To avoid such shortcut and to better evaluate the ability of the model to infer future motions, we further evaluate on a subset of test dataset that contains clear motions. The results on this subset is shown in Tab. 4. In this subset, Copy Last GT no longer achieves good results. Although both Sound2Sight and our method have a large performance drop too, our model can still surpass Sound2Sight by a large margin. This verifies our method is more motion-aware.

AudioSet-Drums. Tab. 3 shows quantitative results on AudioSet-Drums. Our model surpasses others at almost every time step. Similar to YouTube Painting, a model can achieve good results by simply copying last ground truth frame. For fair evaluation, we also select a subset of test videos which exhibit clear motion. The results are shown in Tab. 5. We notice that our superiority is not as obvious on AudioSet-Drums as on other two datasets. The reason may be that motion only exists in a small region of frames in AudioSet Drums, and is hard for our model to fully capture it. Nevertheless, our model still achieves best result.

Method	Type	SSIM ↑				PSNR ↑			
		Fr 16	Fr 30	Fr 45	Mean	Fr 16	Fr 30	Fr 45	Mean
Vougioukas et al. (2018)	M	0.9281	0.9126	0.9027	—	26.97	25.58	24.78	—
Denton and Fergus (2018)	V	0.9779	0.6654	0.4193	—	32.52	16.05	11.84	—
Sound2Sight (Chatterjee and Cherian, 2020) *	M	0.9716	0.9291	0.9110	—	32.73	27.27	25.57	—
Copy Last GT	V	0.9797	0.9250	0.9045	0.9255	36.19	26.90	25.06	27.39
Sound2Sight (Chatterjee and Cherian, 2020) †	M	0.9716	0.9261	0.9074	0.9264	31.91	26.73	25.17	26.95
Our Method	M	0.9848	0.9284	0.9104	0.9313	35.12	27.19	25.53	27.70

Table 2. Comparison on YouTube Painting with 15 seen frames. * denotes highest results from 100x sampling reported in (Chatterjee and Cherian, 2020). † denotes our reproduced average results of (Chatterjee and Cherian, 2020) from 100x sampling.

Method	Type	SSIM ↑				PSNR ↑			
		Fr 16	Fr 30	Fr 45	Mean	Fr 16	Fr 30	Fr 45	Mean
Vougioukas et al. (2018)	M	0.8986	0.8905	0.8866	—	23.62	23.14	22.91	—
Denton and Fergus (2018)	V	0.9706	0.6606	0.5097	—	30.01	16.57	13.49	—
Sound2Sight (Chatterjee and Cherian, 2020) *	M	0.9843	0.9544	0.9466	—	33.24	27.94	26.99	—
Copy Last GT	V	0.9888	0.9464	0.9370	0.9481	35.36	27.08	26.04	27.48
Sound2Sight (Chatterjee and Cherian, 2020) †	M	0.9875	0.9524	0.9434	0.9544	34.23	27.73	26.71	28.13
Our Method	M	0.9896	0.9533	0.9437	0.9558	35.00	27.76	26.68	28.22

Table 3. Comparison on AudioSet-Drums with 15 seen frames. * denotes highest results from 100x sampling reported in (Chatterjee and Cherian, 2020). † denotes our reproduced average results of (Chatterjee and Cherian, 2020) from 100x sampling.

Method		SSIM ↑			
		Fr 16	Fr 30	Fr 45	Mean
Sound2Sight (Chatterjee and Cherian, 2020) †		0.9460	0.8660	0.8429	0.8647
Copy Last GT		0.9499	0.8660	0.8383	0.8609
Our Method		0.9679	0.8701	0.8503	0.8747

Table 4. Comparison on the Clear-Motion Subset of YouTube Painting with 15 seen frames.

Method		SSIM ↑			
		Fr 16	Fr 30	Fr 45	Mean
Sound2Sight (Chatterjee and Cherian, 2020) †		0.9773	0.9086	0.8970	0.9143
Copy Last GT		0.9752	0.8949	0.8854	0.8989
Our Method		0.9807	0.9120	0.8994	0.9180

Table 5. Comparison on the Clear-Motion Subset of Audioset-Drums with 15 seen frames.

4.2. Ablation Study

Effectiveness of audio-motion correlation in MME. As audio is directly influencing the optical flow prediction, we analyze the effectiveness of audio in MME. We compare the quality of optical flow using average endpoint error (AEPE) (Sun et al., 2018; Ilg et al., 2017; Liu et al., 2021) in Tab. 7. The baseline ‘V’ predicts optical flow without audio. ‘V+Recall’ uses audio as motion memory to recall, but does not condense it. ‘MME’ is our full model in stage 1 with both condense memory and recall. MME has the lowest error in the flow prediction. The qualitative comparison is shown in Fig. 7. Although ‘V+Recall’ captures the correct motion in short term, it fails at longer future due to its large-size memory. On the other hand, MME has a better balance in both short-term and long-term predictions. This study proves that audio is effective and our proposed audio motion memory functions well.

Effectiveness of Context-Aware Refinement. We analyze the effects of our proposed CAR in Tab. 6. ‘MME+Unet’ only uses U-Net for refinement in stage 2. ‘MME+Unet+ContextEnc’

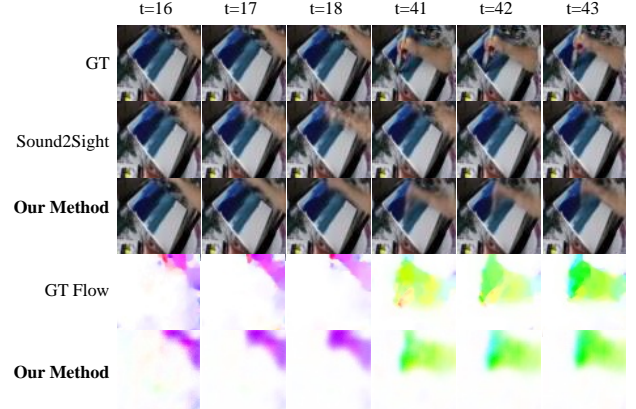


Fig. 6. Qualitative results on YouTube Painting.

adds a context encoder but does not perform affine transformation over the context feature. ‘V+CAR’ uses optical flow predicted without audio. ‘MME+CAR’ is our full model with motion-conditioned affine transformation. We can see from the first and second rows that a single U-Net is insufficient to model image appearance in long-term prediction, and thus it is very important to supply additional context information. The third row illustrates the importance of audio in the optical flow prediction for CAR. In comparison to our full model in the last row, we can see a drop in performance in the third row where the optical flow is predicted without audio. We can see from the second and last rows that our motion conditioned affine transformation is able to adjust the global context feature for better performance in each time step. The qualitative comparison is shown in Fig. 8. CAR is able to provide and aggregate the feature of hand and pen to make the moving object more concrete.

Method	Type	SSIM ↑				PSNR ↑			
		Fr 16	Fr 30	Fr 45	Mean	Fr 16	Fr 30	Fr 45	Mean
MME+Unet	M	0.9873	0.9105	0.8761	0.9143	36.47	25.30	23.15	26.15
MME+Unet+ContextEnc	M	0.9821	0.9266	0.9091	0.9291	34.25	27.06	25.51	27.50
V+CAR	V	0.9834	0.9283	0.9088	0.9296	34.03	26.97	25.32	27.36
MME+CAR	M	0.9848	0.9284	0.9104	0.9313	35.12	27.19	25.53	27.70

Table 6. Analysis of CAR on YouTube Painting.

Method	YouTube	MNIST	AudioSet
V	11.25	—	—
V + Recall	10.43	6.40	4.63
MME	9.85	4.82	3.97

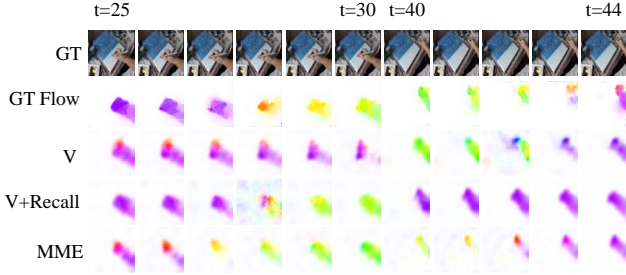
Table 7. Analysis of audio in MME. AEPE results are presented in 10^{-2} scale.

Fig. 7. Qualitative comparison of different motion estimation networks.

5. Conclusions

In this paper, we address the task of audio-visual conditioned video prediction by decoupling it into motion and appearance. We design the MME and CAR by considering the influence of audio and visual modalities in each component. MME leverages audio-motion correlation by using audio as an external motion memory in predicting future optical flow. CAR addresses the loss of appearance context in long term prediction by adding a context encoder. To make the global context feature compatible with motion variance, we perform motion-conditioned affine transformation to adjust the feature. The effectiveness of our proposed method is analyzed both quantitatively and qualitatively.

References

Afouras, T., Owens, A., Chung, J.S., Zisserman, A., 2020. Self-supervised learning of audio-visual objects from video, in: Computer Vision–ECCV 2020: 16th European Conference, Glasgow, UK, August 23–28, 2020, Proceedings, Part XVIII 16, Springer, pp. 208–224.

Arandjelovic, R., Zisserman, A., 2017. Look, listen and learn, in: Proceedings of the IEEE International Conference on Computer Vision, pp. 609–617.

Arandjelovic, R., Zisserman, A., 2018. Objects that sound, in: Proceedings of the European conference on computer vision (ECCV), pp. 435–451.

Aytar, Y., Vondrick, C., Torralba, A., 2016. Soundnet: Learning sound representations from unlabeled video. *Advances in neural information processing systems* 29, 892–900.

Baker, S., Scharstein, D., Lewis, J., Roth, S., Black, M.J., Szeliski, R., 2011. A database and evaluation methodology for optical flow. *International journal of computer vision* 92, 1–31.

Bei, X., Yang, Y., Soatto, S., 2021. Learning semantic-aware dynamics for video prediction, in: Proceedings of the IEEE/CVF Conference on Computer Vision and Pattern Recognition, pp. 902–912.

Chatterjee, M., Cherian, A., 2020. Sound2sight: Generating visual dynamics from sound and context, in: European Conference on Computer Vision, Springer, pp. 701–719.

Chen, H., Xie, W., Afouras, T., Nagrani, A., Vedaldi, A., Zisserman, A., 2021. Localizing visual sounds the hard way, in: Proceedings of the IEEE/CVF Conference on Computer Vision and Pattern Recognition, pp. 16867–16876.

Chen, L., Maddox, R.K., Duan, Z., Xu, C., 2019. Hierarchical cross-modal talking face generation with dynamic pixel-wise loss, in: Proceedings of the IEEE/CVF Conference on Computer Vision and Pattern Recognition, pp. 7832–7841.

Chung, J.S., Jamaludin, A., Zisserman, A., 2017. You said that? *arXiv preprint arXiv:1705.02966*.

Denton, E., Fergus, R., 2018. Stochastic video generation with a learned prior, in: International Conference on Machine Learning, PMLR, pp. 1174–1183.

Gao, R., Chen, C., Al-Halah, Z., Schissler, C., Grauman, K., 2020. Visualechoes: Spatial image representation learning through echolocation, in: European Conference on Computer Vision, Springer, pp. 658–676.

Gao, R., Grauman, K., 2019. Co-separating sounds of visual objects, in: Proceedings of the IEEE/CVF International Conference on Computer Vision, pp. 3879–3888.

Gemmeke, J.F., Ellis, D.P., Freedman, D., Jansen, A., Lawrence, W., Moore, R.C., Plakal, M., Ritter, M., 2017. Audio set: An ontology and human-labeled dataset for audio events, in: 2017 IEEE International Conference on Acoustics, Speech and Signal Processing (ICASSP), IEEE, pp. 776–780.

Hu, D., Nie, F., Li, X., 2019. Deep multimodal clustering for unsupervised audiovisual learning, in: Proceedings of the IEEE/CVF Conference on Computer Vision and Pattern Recognition, pp. 9248–9257.

Hu, D., Qian, R., Jiang, M., Tan, X., Wen, S., Ding, E., Lin, W., Dou, D., 2020. Discriminative sounding objects localization via self-supervised audiovisual matching. *Advances in Neural Information Processing Systems* 33.

Ilg, E., Mayer, N., Saikia, T., Keuper, M., Dosovitskiy, A., Brox, T., 2017. Flownet 2.0: Evolution of optical flow estimation with deep networks, in: Proceedings of the IEEE conference on computer vision and pattern recognition, pp. 2462–2470.

Jaderberg, M., Simonyan, K., Zisserman, A., et al., 2015. Spatial transformer networks. *Advances in neural information processing systems* 28, 2017–2025.

Jin, B., Hu, Y., Tang, Q., Niu, J., Shi, Z., Han, Y., Li, X., 2020. Exploring spatial-temporal multi-frequency analysis for high-fidelity and temporal-consistency video prediction, in: Proceedings of the IEEE/CVF Conference on Computer Vision and Pattern Recognition, pp. 4554–4563.

Kingma, D.P., Ba, J., 2014. Adam: A method for stochastic optimization. *arXiv preprint arXiv:1412.6980*.

Knöpfel, T., Sweeney, Y., Radulescu, C.I., Zabouri, N., Doostdar, N., Clopath, C., Barnes, S.J., 2019. Audio-visual experience strengthens multisensory assemblies in adult mouse visual cortex. *Nature communications* 10, 1–15.



Fig. 8. Qualitative comparison of different refinement networks.

Korbar, B., Tran, D., Torresani, L., 2018. Cooperative learning of audio and video models from self-supervised synchronization. arXiv preprint arXiv:1807.00230 .

Lee, A.X., Zhang, R., Ebert, F., Abbeel, P., Finn, C., Levine, S., 2018. Stochastic adversarial video prediction. arXiv preprint arXiv:1804.01523 .

Lee, S., Kim, H.G., Choi, D.H., Kim, H.I., Ro, Y.M., 2021a. Video prediction recalling long-term motion context via memory alignment learning, in: Proceedings of the IEEE/CVF Conference on Computer Vision and Pattern Recognition, pp. 3054–3063.

Lee, W., Jung, W., Zhang, H., Chen, T., Koh, J.Y., Huang, T., Yoon, H., Lee, H., Hong, S., 2021b. Revisiting hierarchical approach for persistent long-term video prediction. arXiv preprint arXiv:2104.06697 .

Liu, P., Lyu, M.R., King, I., Xu, J., 2021. Learning by distillation: A self-supervised learning framework for optical flow estimation. IEEE Transactions on Pattern Analysis and Machine Intelligence .

Morgado, P., Vasconcelos, N., Misra, I., 2021. Audio-visual instance discrimination with cross-modal agreement, in: Proceedings of the IEEE/CVF Conference on Computer Vision and Pattern Recognition, pp. 12475–12486.

Owens, A., Efros, A.A., 2018. Audio-visual scene analysis with self-supervised multisensory features, in: Proceedings of the European Conference on Computer Vision (ECCV), pp. 631–648.

Reed, S.E., Zhang, Y., Zhang, Y., Lee, H., 2015. Deep visual analogy-making. Advances in neural information processing systems 28, 1252–1260.

Ronneberger, O., Fischer, P., Brox, T., 2015. U-net: Convolutional networks for biomedical image segmentation, in: International Conference on Medical image computing and computer-assisted intervention, Springer. pp. 234–241.

Senocak, A., Oh, T.H., Kim, J., Yang, M.H., Kweon, I.S., 2018. Learning to localize sound source in visual scenes, in: Proceedings of the IEEE Conference on Computer Vision and Pattern Recognition, pp. 4358–4366.

Srivastava, N., Mansimov, E., Salakhudinov, R., 2015. Unsupervised learning of video representations using lstms, in: International conference on machine learning, PMLR. pp. 843–852.

Sun, D., Yang, X., Liu, M.Y., Kautz, J., 2018. Pwc-net: Cnns for optical flow using pyramid, warping, and cost volume, in: Proceedings of the IEEE conference on computer vision and pattern recognition, pp. 8934–8943.

Tao, M., Tang, H., Wu, S., Sebe, N., Jing, X.Y., Wu, F., Bao, B., 2020. Dfgan: Deep fusion generative adversarial networks for text-to-image synthesis. arXiv preprint arXiv:2008.05865 .

Tian, Y., Li, D., Xu, C., 2020. Unified multisensory perception: Weakly-supervised audio-visual video parsing, in: Computer Vision–ECCV 2020: 16th European Conference, Glasgow, UK, August 23–28, 2020, Proceedings, Part III 16, Springer. pp. 436–454.

Villegas, R., Erhan, D., Lee, H., et al., 2018. Hierarchical long-term video prediction without supervision, in: International Conference on Machine Learning, PMLR. pp. 6038–6046.

Villegas, R., Yang, J., Zou, Y., Sohn, S., Lin, X., Lee, H., 2017. Learning to generate long-term future via hierarchical prediction, in: international conference on machine learning, PMLR. pp. 3560–3569.

Vougioukas, K., Petridis, S., Pantic, M., 2018. End-to-end speech-driven facial animation with temporal gans. arXiv preprint arXiv:1805.09313 .

Wang, T.C., Liu, M.Y., Zhu, J.Y., Liu, G., Tao, A., Kautz, J., Catanzaro, B., 2018a. Video-to-video synthesis, in: Proceedings of the 32nd International Conference on Neural Information Processing Systems, pp. 1152–1164.

Wang, Y., Jiang, L., Yang, M.H., Li, L.J., Long, M., Fei-Fei, L., 2018b. Ei-detic 3d lstm: A model for video prediction and beyond, in: International conference on learning representations.

Wang, Y., Long, M., Wang, J., Gao, Z., Yu, P.S., 2017. Predrnn: Recurrent neural networks for predictive learning using spatiotemporal lstms, in: Proceedings of the 31st International Conference on Neural Information Processing Systems, pp. 879–888.

Wang, Z., Bovik, A.C., Sheikh, H.R., Simoncelli, E.P., 2004. Image quality assessment: from error visibility to structural similarity. IEEE transactions on image processing 13, 600–612.

Wu, Y., Gao, R., Park, J., Chen, Q., 2020. Future video synthesis with object motion prediction, in: Proceedings of the IEEE/CVF Conference on Computer Vision and Pattern Recognition, pp. 5539–5548.

Wu, Y., Yang, Y., 2021. Exploring heterogeneous clues for weakly-supervised audio-visual video parsing, in: Proceedings of the IEEE/CVF Conference on Computer Vision and Pattern Recognition, pp. 1326–1335.

Xingjian, S., Chen, Z., Wang, H., Yeung, D.Y., Wong, W.K., Woo, W.c., 2015. Convolutional lstm network: A machine learning approach for precipitation nowcasting, in: Advances in neural information processing systems, pp. 802–810.

Yang, K., Russell, B., Salamon, J., 2020. Telling left from right: Learning spatial correspondence of sight and sound, in: Proceedings of the IEEE/CVF Conference on Computer Vision and Pattern Recognition, pp. 9932–9941.

Yin, Z., Shi, J., 2018. Geonet: Unsupervised learning of dense depth, optical flow and camera pose, in: Proceedings of the IEEE conference on computer vision and pattern recognition, pp. 1983–1992.

Zach, C., Pock, T., Bischof, H., 2007. A duality based approach for realtime tv-l 1 optical flow, in: Joint pattern recognition symposium, Springer. pp. 214–223.

Zhao, H., Gan, C., Ma, W.C., Torralba, A., 2019. The sound of motions, in: Proceedings of the IEEE/CVF International Conference on Computer Vision, pp. 1735–1744.

Zhao, H., Gan, C., Rouditchenko, A., Vondrick, C., McDermott, J., Torralba, A., 2018. The sound of pixels, in: Proceedings of the European conference on computer vision (ECCV), pp. 570–586.

Zhou, H., Liu, Y., Liu, Z., Luo, P., Wang, X., 2019. Talking face generation by adversarially disentangled audio-visual representation, in: Proceedings of the AAAI Conference on Artificial Intelligence, pp. 9299–9306.

Supplementary Material

Appendix A. Clear-Motion Subset

We observe that large portions of existing benchmarks videos consist of small or no motion. For better evaluation, we select subsets of videos with obvious motions. A clear-motion video is determined by the average maximum magnitude of its optical flows. A video is considered as clear-motion if the average maximum magnitude is above 1.5 pixels. Tab. A.8 shows the number of videos before and after selection. ‘thr=0’ is the full test dataset. ‘thr=1.5’ is the clear-motion subset.

Dataset	thr=0	thr=1.5
YouTube Painting	500	148
AudioSet-Drums	1000	233

Table A.8. The number of test videos before and after selection.

Appendix B. Architecture Details

We present the detailed architecture of our proposed framework.

Motion Encoder. The motion encoder consists of four convolutional layers with kernel size of 4×4 and stride of 2. The number of channels is $\{64, 64, 128, 128\}$. Each convolutional layer is followed by Batch Normalization and Leaky ReLU, except for the last layer which is followed by Batch Normalization and Tanh.

Motion Decoder. The motion decoder consists of four deconvolution layers with kernel size of 4×4 and stride of 2. The number of channels is $\{128, 64, 64, 2\}$. Each convolutional layer is followed by Batch Normalization and Leaky ReLU, except for the last layer.

Audio Encoder. The audio encoder consists of five convolutional layers with kernel size of 4×4 for the first four layers and with kernel size of 2×2 for the last layer. The number of channels is $\{64, 128, 256, 512, 128\}$. Each convolutional layer is followed by Batch Normalization and Leaky ReLU, except for the last layer which is followed by Batch Normalization and Tanh.

Condense and Recall. The operators Condense and Recall use attention mechanism as shown in Fig B.9. Specifically, Operator Condense takes the motion memory MM as input and projects it into the query (Q), key (K) and value (V) via three separate 1D convolutional layers with kernel size of 1, respectively. In Recall, the visual feature is sent into a 2D convolutional layer with kernel size of 1×1 and then is flattened along spatial dimensions as Q . The condensed memory is sent into two separate 1D convolutional layers with kernel size of 1 and projected as K and V , respectively.

Context Encoder. The context encoder has four blocks, where each block consists of two convolutional layers followed by Batch Normalization and ReLU. A max pooling layer is inserted between adjacent blocks.

AffBlock. Fig B.10 shows the architecture of AffBlock. Each AffBlock contains twice motion-conditioned affine transformation. It has one convolutional layer with kernel size of 3×3 and stride of 1 at the end of the block.

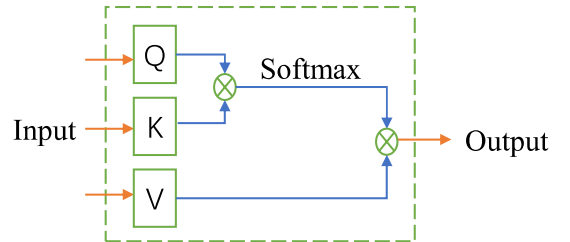


Fig. B.9. Illustration of the attention mechanism.

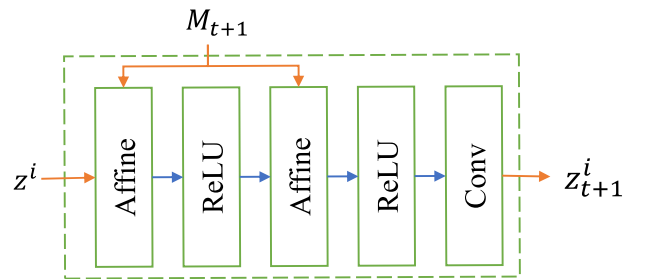


Fig. B.10. Architecture of the AffBlock.